


Visualizing molecular orientational ordering and electronic structure in Cs_nC_{60} fulleride filmsSha Han,¹ Meng-Xue Guan,² Can-Li Song ^{1,3,*}, Yi-Lin Wang,⁴ Ming-Qiang Ren,¹ Sheng Meng,² Xu-Cun Ma,^{1,3,†} and Qi-Kun Xue^{1,3,5}¹State Key Laboratory of Low-Dimensional Quantum Physics, Department of Physics, Tsinghua University, Beijing 100084, China²Institute of Physics, Chinese Academy of Sciences, Beijing 100190, China³Frontier Science Center for Quantum Information, Beijing 100084, China⁴Center of Nanoelectronics and School of Microelectronics, Shandong University, Jinan 250100, China⁵Beijing Academy of Quantum Information Sciences, Beijing 100193, China

(Received 20 November 2019; accepted 3 February 2020; published 20 February 2020)

Alkali-doped fullerides exhibit a wealth of unusual phases that remain controversial by nature. Here we report a cryogenic scanning tunneling microscopy study of the submolecular structural and electronic properties of expanded fullerene C_{60}^{n-} films with various cesium dopings. By varying the discrete charge states and film thicknesses, we reveal a large tunability of orientational ordering of C_{60}^{n-} anions, yet the tunneling conductance spectra are all robustly characteristic of energy gaps, hallmarks of Jahn-Teller instability and electronic correlations. The Fermi level lies halfway within the insulating gap for stoichiometric Cs doping level of $n = 1, 2, 3,$ and $4,$ apart from which it moves toward band edges with concomitant electronic states within the energy gap. Our findings establish the universality of Jahn-Teller instability and clarify the relationship between the doping and structural and electronic properties in Cs_nC_{60} fullerides.

DOI: [10.1103/PhysRevB.101.085413](https://doi.org/10.1103/PhysRevB.101.085413)**I. INTRODUCTION**

Emergent phenomena and exotic electronic phases in organic molecular solids, including superconductivity [1–4], magnetism [5,6], charge [7], and orientational ordering [8–12], have been routinely explored in condensed-matter physics, as well as for potential applications in electronics [13]. Alkali-doped fullerides (A_3C_{60}), for example, exhibit superconductivity with a maximum transition temperature $T_c \sim 40$ K and have brought about special interest in the superconductivity research community [14–19] because they exhibit a proximity magnetic Mott-insulating state accompanied by the dome-shaped dependence of superconductivity upon pressure or chemical doping in common with unconventional high- T_c superconductors of the cuprate and ferropnictide classes [20,21]. A minor but significant distinction is the unique occurrence of on-molecule electron-vibration coupling in fullerides, which might lift the active t_{1u} orbital degeneracy of spherical C_{60}^{n-} anions via Jahn-Teller (JT) distortions and competes with local exchange coupling [22,23], thereby leading to an orbital disproportionation of filled electrons [24–28]. The complexity associated with comparable bandwidth to the energy scale of on-molecule electron-phonon coupling and electronic correlations (characterized by the Hubbard U) renders it nontrivial to perceive comprehensively the fundamental electronic structure and microscopic mechanism of fulleride superconductivity on the verge of Mott localization [29].

On the other hand, the C_{60} molecules are orientationally disordered in the fcc trivalent fulleride superconductors A_3C_{60}

($A = K, Rb,$ and Cs) [1,4,14–18]. These merohedral disorders could also affect the electronic structure and properties that appear unique to molecular solids [24,30]. Furthermore, the molecular orientation depends substantially on the charge state of the C_{60}^{n-} anions [31–34]. Thus, it becomes increasingly significant to determine experimentally the doping dependence of the molecular configuration and fundamental electronic structure that are essential prerequisites for understanding the novel properties of fullerene-based solids.

Cesium-doped fullerides are particularly fascinating because the most expanded crystal structure leads to a relatively small intermolecular hopping. This serves as a model system to understand the interplay between the competing intramolecular interactions and therefore ground states in the orbitally degenerate fulleride families. However, the sample imperfections and phase separation in this category of materials have largely frustrated a clear-cut relationship between the composition stoichiometry and electronic structure [14–18]. Local probes may circumvent this issue but thus far have been limited to a few underdoped K_nC_{60} thin films (n is the doping concentration) on metal substrates [9,31,32], where the substrate screening effects play an important role in the electronic structure of fullerides. Here we actualize systematic doping control of the expanded Cs_nC_{60} fulleride films on graphitized SiC(0001) substrates that allows us to track the doping-dependent submolecular configuration and fundamental electronic structure by means of scanning tunneling microscopy (STM). Despite the diversity of molecular orientational ordering, the electronic ground states are all insulating in Cs_nC_{60} fullerides, with integer $n = 1, 2, 3$ and $4,$ which we ascribe to the cooperative interplay between the on-molecule Jahn-Teller distortions and electronic correlations.

*Corresponding author: clsong07@mail.tsinghua.edu.cn†Corresponding author: xucunma@mail.tsinghua.edu.cn

II. EXPERIMENTAL METHODS

All experiments were carried out in an ultrahigh-vacuum, low-temperature STM system equipped with a molecular beam epitaxy (MBE) chamber for *in situ* sample preparation. The base pressure of both MBE and STM chambers is better than 1.0×10^{-10} Torr. Monolayer and multilayer fullerene epitaxial thin films were prepared in the MBE chamber by thermal evaporation of the C_{60} source out of a standard Knudsen cell on graphitized SiC(0001) substrates with a resistivity of $\sim 0.1 \Omega \text{ cm}$. Evaporation of desired equivalents of Cs onto the pristine C_{60} films from a thoroughly outgassed SAES getter at room temperature followed by moderate annealing at $\sim 473 \text{ K}$ yields electron-doped $Cs_n C_{60}$ films with a well-controlled doping level n . Here the flux rates of C_{60} and Cs sources are estimated by separately depositing them onto a clean graphene substrate at a cryogenic temperature of approximately 100 K and counting the number of C_{60} molecules or Cs from STM images. The calculated ratio of flux and growth duration for Cs and C_{60} are used to determine the nominal Cs doping in Cs-doped fullerene films.

After MBE growth, the fulleride films were *in situ* transferred into the STM head for topographic imaging and electronic structure measurements at 4.8 K. Polycrystalline PtIr tips were precleaned by *e*-beam heating, calibrated on MBE-grown Ag films, and used throughout the experiments. All STM topographies were acquired in a constant-current mode with the bias voltage V applied to the sample. Tunneling spectra were measured using the standard lock-in technique with a small bias modulation of 20 meV at 987.5 Hz.

III. RESULTS AND DISCUSSION

A. STM characterization of undoped C_{60}

As a substrate, graphene has unique superiority in that it decouples effectively the C_{60} overlayer from the underlying substrates and enables us to deduce readily the innate character of alkali fullerides [12,35]. Figure 1(a) depicts the large-scale STM topography of pristine (undoped) C_{60} films on graphene, assembled into a (111)-orientated fcc crystal structure. We observe the coexistence of monolayer, bilayer, and multilayer C_{60} films as well as the graphene/SiC surface (see also the inset). Regardless of layer indexing, the fullerenes are closely packed into hexagonal structure with an intermolecular spacing d of $10.0 \pm 0.1 \text{ \AA}$ [Figs. 1(b) and 1(c)], consistent with previous reports [10–12,31,32,35]. The submolecular structure, however, reveals complex configurations of C_{60} molecules with respect to the surface. As is typical for fullerene in a spherical basis, five distinct orientations, with a hexagon (H), a pentagon (P), a 6:6 bond (H:H), a 6:5 bond (H:P), and a carbon apex (CA) pointing up, have been routinely observed in experiments [10–12,36] and are drawn schematically in Fig. 1(d). Here the H:H bonds between two hexagons exhibit a double-bond character, while the H:P bonds separating pentagons and hexagons have a prevalent single-bond character. Given that the 6:5 bonds have relatively lower electron density and the C_{60} pentagons brighten in the empty-state STM topography, one can readily distinguish the orientations of C_{60} by symmetry and can typically superimpose them onto the corresponding C_{60} molecules in

Figs. 1(b) and 1(c). Apparently, the C_{60} molecules with tristar and two-lobe intramolecular structures in Fig. 1(c) correspond to the H and H:H orientations, namely, with the hexagon and 6:6 bond facing the surface, respectively, whereas for the third kind of C_{60} orientation the brightest spots are always found to be off center from the C_{60} center (see the coaxial circles and dots). We therefore reasonably assign them as H:P orientation, and the bright spots are characteristic of the pentagons. In Fig. 1(b), except for the H:P-orientated C_{60} , other dim molecules are then assigned as P-orientated C_{60} . This is understandable since a C_{60} molecule with its bond facing up is higher than that with the pentagon ring facing up. Energetically, considering that electron-doped graphene will preferentially transfer electrons to an undoped C_{60} monolayer, the P orientation is more favorable as well.

Careful scrutiny of molecular-resolved STM images reveals a certain regularity in the molecular orientations. For example, the H-oriented C_{60} molecules in the second layer arrange well into a quasi- (2×2) superstructure relative to the intermolecular spacing, marked by the white rhombus in Fig. 1(c). The reason why we call it a quasi- (2×2) superstructure is that the other C_{60} molecules exhibit no long-range order in view of the molecular orientations. Likewise, the local 2×2 superstructure in the H:P orientation, albeit faint, develops on the C_{60} monolayer [Fig. 1(b)]. The ordering of molecular orientation is further evidenced by fast Fourier transform (FFT) patterns inserted in Figs. 1(b) and 1(c), which, in addition to lattice Bragg spots, exhibit extra spots from the quasi- (2×2) superstructure of the molecular orientation, circled by the dashed lines.

Figure 1(e) depicts the typical differential conductance dI/dV spectrum measured on the monolayer C_{60} films. The peaks at -2.7 , 0.8 , and 2.3 eV correspond to the highest occupied molecular orbital (HOMO), the lowest unoccupied molecular orbital (LUMO), and the LUMO + 1 states of C_{60} fullerene, respectively. A larger HOMO-LUMO gap of 3.5 eV reconciles fairly well with negligible electrostatic screening from the underlying graphene substrate [12,35], in marked contrast to fullerenes grown on metal surface [37,38]. Yet it is worth noting that the triply degenerate t_{1u} LUMO and t_{1g} LUMO + 1 levels split individually into two discrete peaks, a hallmark of JT distortion in charged fullerenes [inset of Fig. 1(e)] [39,40]. Here the charging of C_{60} is prompted by electron transfer from graphene, owing to a large electron affinity of fullerene [41]. This appears to be in good agreement with the tunneling spectrum where the Fermi level E_F lies closer to the LUMO [Fig. 1(e)].

B. Orientational ordering in $Cs_n C_{60}$

We highlight that the molecular orientational ordering is closely associated with the charge state of fullerenes (see the Appendix), as convincingly rationalized by a systematic survey of $Cs_n C_{60}$ films on the submolecular scale. Figures 2 and 3 show STM topographies and electronic structures of $Cs_n C_{60}$ films ($n = 1, 2, 3$, and 4) as functions of the film thickness and electron doping $n-$. Upon further doping, the excess Cs atoms cluster together on the overlayer [Fig. 4(a)]. A comparison among STM topographies reveals that the configuration of C_{60}^{n-} anions is

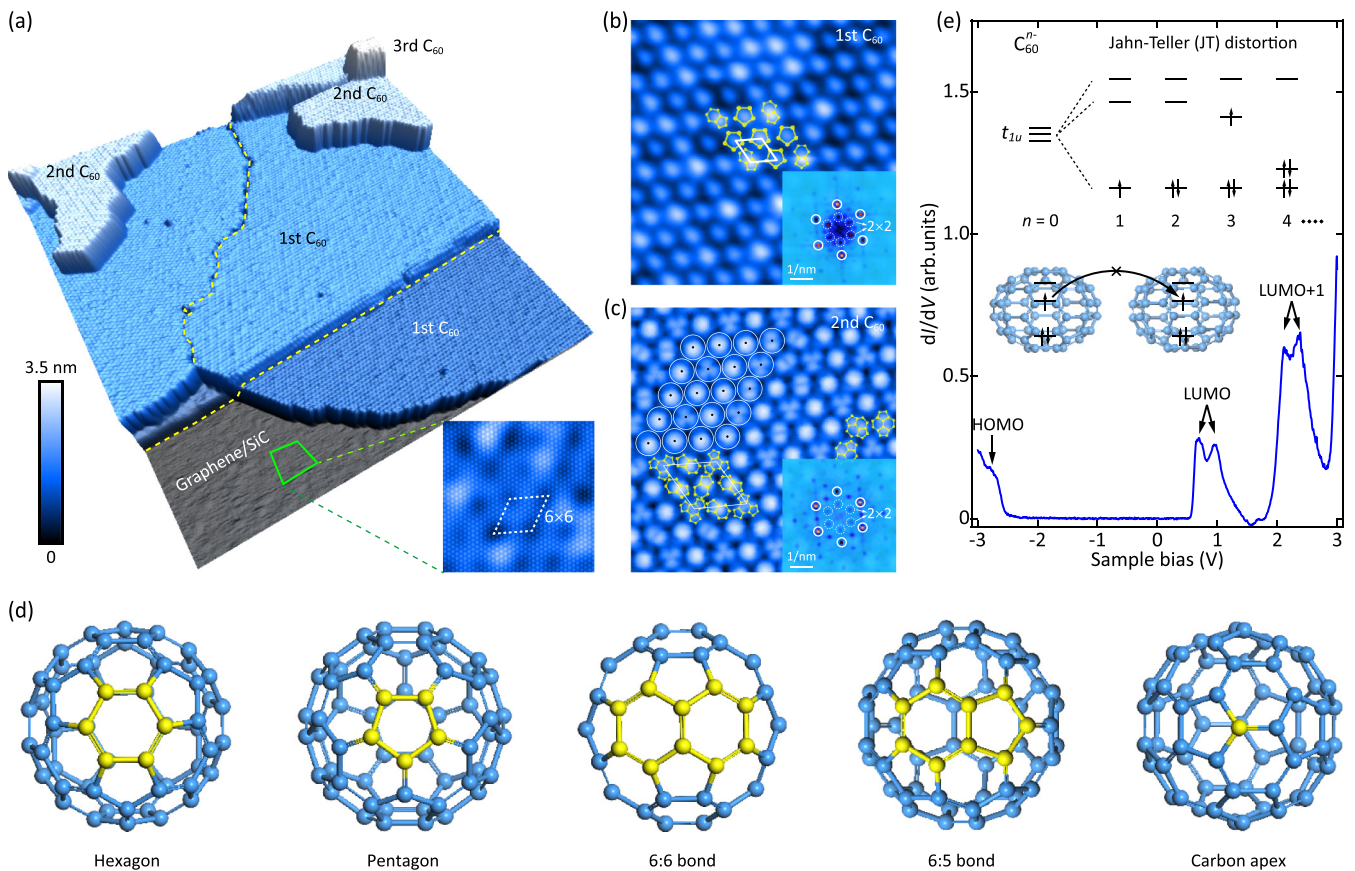


FIG. 1. Characterization of pristine C_{60} fullerenes on graphene. (a) STM topography ($100 \times 100 \text{ nm}^2$) of as-grown C_{60} thin films taken with sample bias $V = 3.0 \text{ V}$ and tunneling current $I = 200 \text{ pA}$. Color-coded plateaus reveal four distinct regions: the C_{60} -free graphene/SiC surface (gray) and the first layer (blue), second layer (light cyan), and third layer (white) of C_{60} fullerenes. The yellow dashed lines designate two steps from the substrate. The inset shows zoom-in STM topography ($8 \times 8 \text{ nm}^2$, $V = 50 \text{ mV}$, $I = 100 \text{ pA}$) of bilayer graphene on SiC showing the well-known 6×6 superstructure (dashed rhombus). (b) and (c) High-resolution STM images ($10 \times 10 \text{ nm}^2$) of monolayer and bilayer C_{60} films. The insets display the corresponding FFT patterns. Bright spots circled by the solid and dashed lines stem from the self-assembled C_{60} lattice and quasi- (2×2) superstructure in the molecular orientation, respectively. The white rhombus marks the surface unit cell. According to the overlaid lattice mesh (coaxial circles and dots) in (c), the brightest C_{60} molecules are H:P orientated with the pronounced DOS (i.e., pentagon) deviating from the centers of fullerenes. Tunneling conditions are (b) $V = 1.0 \text{ V}$, $I = 100 \text{ pA}$ and (c) $V = 2.0 \text{ V}$, $I = 100 \text{ pA}$. (d) Ball and stick diagrams of C_{60} in the hexagon, pentagon, 6:6 bond, 6:5 bond, and carbon apex orientations, from left to right. (e) Representative conductance dI/dV spectrum of C_{60} films on graphene, with a set point of $V = 1.0 \text{ V}$ and $I = 100 \text{ pA}$. The splitting of triply degenerate t_{1u} LUMO and t_{1g} LUMO + 1 levels is due to the JT distortion of icosahedral symmetric C_{60} molecules upon electron doping of fullerene. The inset shows modified molecular orbitals (top) of C_{60}^{n-} anions by JT distortion (bottom), with its magnitude exaggerated in the molecule model. The up and down arrows denote the up- and down-spin electrons, respectively.

hypersensitive to the charge state $n-$ and film thickness. First, a noteworthy observation is the two-hooklike intramolecular structure with different strengths in bilayer CsC_{60} [Fig. 3(a)], which matches the CA-oriented fullerenes in Fig. 1(d). Thus, all five configurations of C_{60} molecules have been convincingly identified in our study. More remarkably, we reveal that the $n-$ charged fullerenes ($n = 1-3$) are consistently H orientated in monolayer Cs_nC_{60} [Figs. 2(a)–2(c)], whereas the molecular configurations change from CA, H:P, and H to H:H with increasing $n = 1-4$ in bilayer Cs_nC_{60} [Figs. 3(a)–3(d)]. This suggests that the graphene- C_{60} interactions, albeit small, cannot be ignored completely in monolayer Cs_nC_{60} . Nevertheless, the C_{60}^{n-} anions all exhibit intriguing molecular orientational ordering, despite it being short range in monolayer CsC_{60} [Fig. 2(a)]. A closer inspection of the submolecular

C_{60} structure reveals the presence of merohedral disorders in stoichiometric Cs_nC_{60} fullerenes except for bilayer Cs_4C_{60} . Evidently, the merohedrally disordered molecules arrange into 1×2 and $\sqrt{3} \times \sqrt{3}$ superstructures in monolayer Cs_2C_{60} [Fig. 2(b)] and Cs_3C_{60} [Fig. 2(c)], whereas no superstructure associated with the merohedral disorders exists in monolayer CsC_{60} [Fig. 2(a)] and bilayer Cs_nC_{60} ($n = 1-4$) [Figs. 3(a)–3(c)].

Apart from stoichiometry with a noninteger ratio between Cs and C_{60} constituents, the orientations of C_{60} anions become spatially disordered, and the molecular ordering vanishes [Fig. 4(b)]. We thus arrive at our first major finding: the molecular orientations of C_{60}^{n-} anions become ordered solely for stoichiometric Cs_nC_{60} compounds with integer n , including zero. Such a finding agrees quite nicely with the local

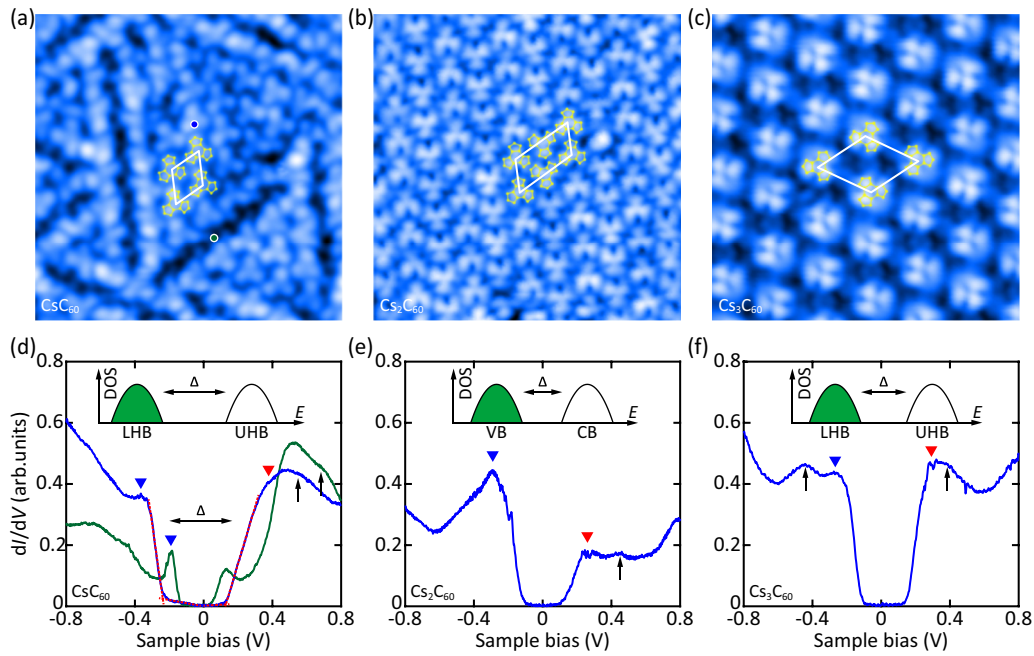


FIG. 2. Orientational ordering and electronic structure in monolayer $Cs_n C_{60}$ for $n = 1-3$. (a)–(c) STM topographic images ($10 \times 10 \text{ nm}^2$) and (d)–(f) tunneling dI/dV spectra (set point: $V = 0.5 \text{ V}$, $I = 100 \text{ pA}$) of monolayer C_{60}^{n-} anions with various Cs dopings as indicated. Tunneling conditions are (a) $V = 1.0 \text{ V}$, $I = 100 \text{ pA}$, (b) $V = -1.0 \text{ V}$, $I = 100 \text{ pA}$, and (c) $V = 0.65 \text{ V}$, $I = 100 \text{ pA}$. The two different spectra in (d) are acquired at the color-coded positions (dots) in (a). Note that the H-orientated fullerenes form a 1×2 superstructure and a $\sqrt{3} \times \sqrt{3}$ superstructure in monolayer $Cs_2 C_{60}$ and $Cs_3 C_{60}$, respectively. Inserted in (d)–(f) are schematic band structures of doped fullerenes with only the LHB/VB (green) and UHB/CB (unfilled) shown, matching nicely with the measured conductance spectra. Onsets of unoccupied (UHB/CB) and occupied (LHB/VB) bands are extracted from the intersections of linear fits to the spectral weights just above and below the corresponding band edges, as exemplified by the red dashes in (d). The up arrows denote satellite peaks from JT distortions. The same convention is used throughout.

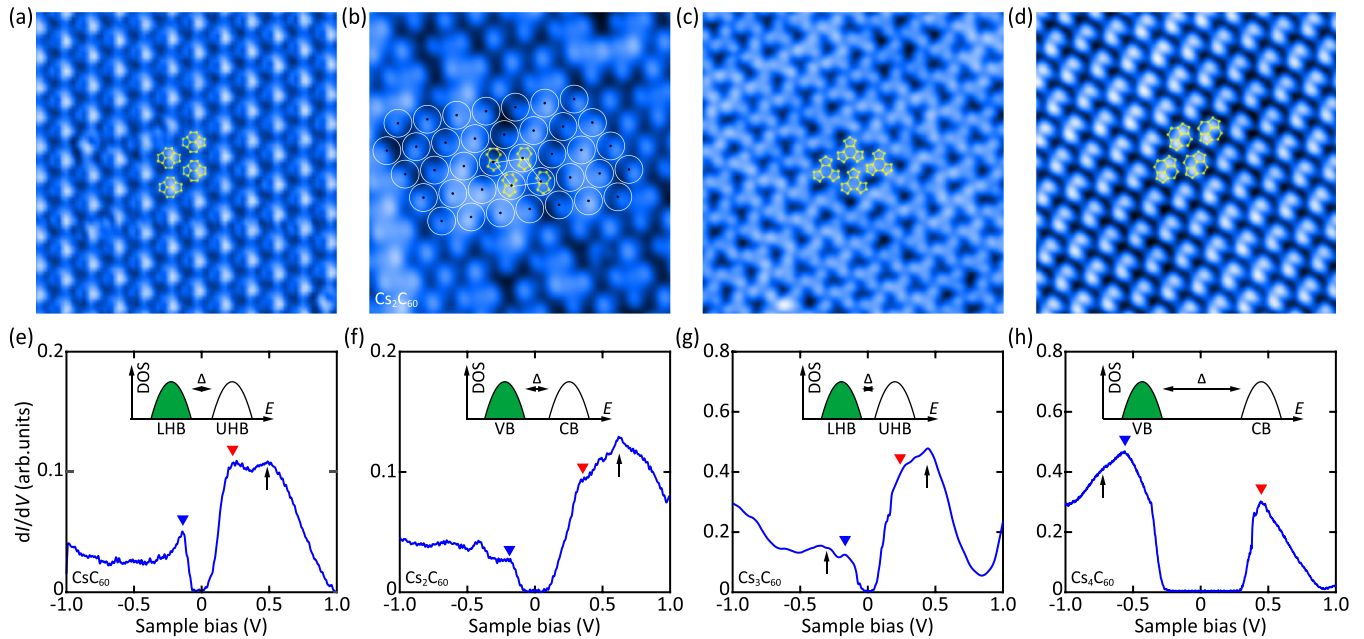


FIG. 3. Orientational ordering and electronic structure in bilayer $Cs_n C_{60}$ for $n = 1-4$. (a)–(d) STM topographic images ($10 \times 10 \text{ nm}^2$) and (e)–(h) tunneling dI/dV spectra of bilayer C_{60}^{n-} anions with various Cs dopings as indicated. Set point: $V = 1.0 \text{ V}$, $I = 100 \text{ pA}$. The molecular orientational ordering is robustly found, but the configuration of C_{60}^{n-} anions shows dramatic dependence on the charge state $n-$, adopting CA, H:P, H, and H:H orientations from $n = 1$ to $n = 4$. Analogous to the undoped C_{60} bilayer, the brightest pentagons in (b) are off center and do not conform to a complete hexagonal lattice, so we assign them to H:P-orientated ordering of C_{60} .

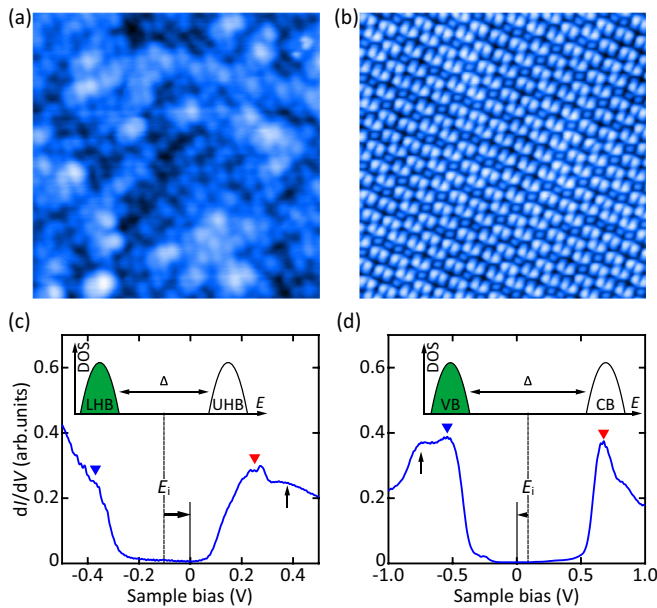


FIG. 4. Structure and electronic DOS in the off-stoichiometric $Cs_n C_{60}$ films. (a) Topography ($20 \times 20 \text{ nm}^2$, $V = 1.0 \text{ V}$, $I = 100 \text{ pA}$) and (c) conductance dI/dV spectrum ($V = 0.7 \text{ V}$, $I = 100 \text{ pA}$) of monolayer $Cs_3 C_{60}$ with excess Cs doping. The configuration of C_{60}^{n-} is indiscernible due to the clustering of excess Cs. (b) Topography ($15 \times 15 \text{ nm}^2$, $V = 1.0 \text{ V}$, $I = 100 \text{ pA}$) and (d) dI/dV spectrum ($V = 1.0 \text{ V}$, $I = 100 \text{ pA}$) of bilayer $Cs_4 C_{60}$ with a deficiency $\delta \sim 0.06$ of Cs. Here δ is estimated as the relative proportion of non-H:H-orientated fullerenes in (b). E_F moves upwards (right arrow) and downwards (left arrow) relative to E_i in (c) and (d), consistent with n - and p -type doping, respectively.

orientational ordering in $K_3 C_{60}$ [31,32], as well as the preference of molecular orientational ordering in pristine C_{60} multilayers [10,11,36,42] or thin films supported by chemically inert substrates [12,43]. In the latter situations, the C_{60} assemblies in question are only limitedly affected by the substrates and conserve their charge neutrality.

We suggest that the intermolecular Coulomb repulsive interactions between charged C_{60}^{n-} anions play a key role in stabilizing the long-range ordering of the molecular orientational ordering observed here. The missing molecular ordering in nonstoichiometric $Cs_n C_{60}$ [Fig. 4(b)] is most likely because the charge states of each fullerene are different and the repulsive forces between them become spatially nonuniform. Further theoretical simulation is desired to thoroughly understand the observed molecular orientational ordering of C_{60}^{n-} anions with varying film thickness and charge state [44].

C. Absence of metallicity in $Cs_n C_{60}$

Having established the diversities of molecular orientations and their ordering in $Cs_n C_{60}$, we explore below the charge state and layer-dependent electronic density of states (DOS) around E_F in Figs. 2(d)–2(f) (monolayer $Cs_n C_{60}$, $n = 1$ –3) and Figs. 3(e)–3(h) (bilayer $Cs_n C_{60}$, $n = 1$ –4). Despite something of a distinction between H-orientated C_{60} domains and the boundaries separating them in monolayer CsC_{60} [Fig. 2(d)], the spatially resolved differential conductance

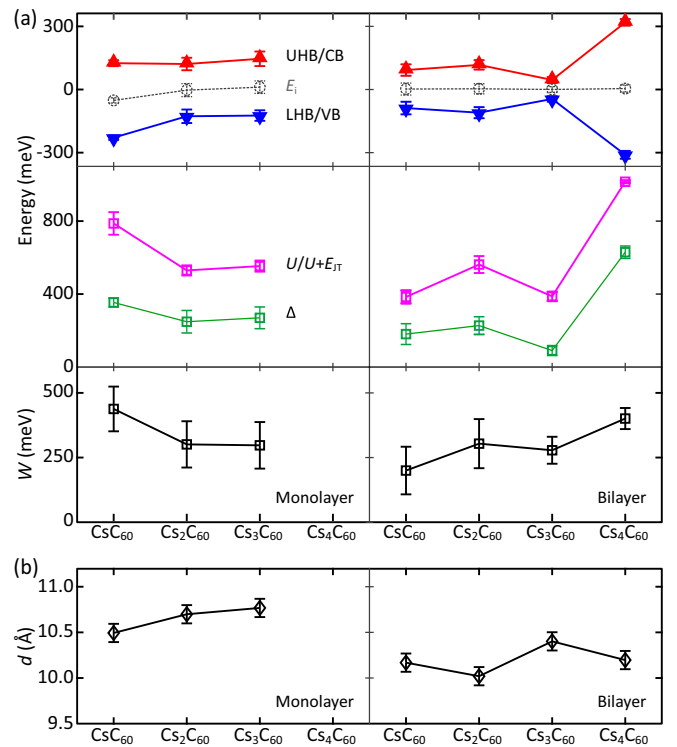


FIG. 5. Energy-band parameters and intermolecular spacing. (a) Onset energies of LHB/VB and UHB/CB (top panel) and $U/U + E_{JT}$ and band gap Δ (middle panel), as well as bandwidth W (bottom panel) in monolayer and bilayer $Cs_n C_{60}$ with varied n . Dashed circles denote the midgap energy E_i , half way between the UHB/CB and LHB/VB edges. (b) Dependence of intermolecular spacing d on the doping level n – and layer index. The errors indicate the standard deviations from multiple dI/dV measurements in (a) or STM calibration uncertainty of $< 0.1 \text{ \AA}$ in (b).

dI/dV spectra are homogeneous in $Cs_n C_{60}$ fullerides with long-range orientational orders. Regardless, all the tunneling spectra present an apparent energy gap in the vicinity of E_F , consistent with insulating electronic states for $Cs_n C_{60}$ fullerides with integer n . This constitutes our second major finding. It is also worth noting that the gaps exist robustly in the off-stoichiometric $Cs_n C_{60}$ fullerides [Figs. 4(c) and 4(d)]. In order to extract the energy gap, we have reasonably determined the onsets of the lowest unoccupied (marked by red triangles) and the highest occupied bands (blue triangles) as the intersections of linear fits to spectral DOS just above and below every band (red dashes) in all dI/dV spectra.

In Fig. 5(a), we plot the onset energies (top panel) and extracted band gap Δ (middle panel) between them versus n and film thickness of $Cs_n C_{60}$. Evidently, Δ not only varies with the charge state n – but also relies critically on film thickness. Despite such alteration, E_F lies close to the midgap energy E_i in $Cs_n C_{60}$ with long-range orientational orders, justified by the gray circles in the top panels of Fig. 5(a). Moving to monolayer CsC_{60} [Fig. 2(d)] and off-stoichiometric fullerides (Fig. 4), however, we see a dramatic change: the Fermi level deviates from E_i and moves upwards (right arrow) or downwards (left arrow), signifying n -type and p -type doping, respectively. Followed by the shift of E_F , a finite

low-lying electronic state develops within the energy gap. This contradicts the stoichiometric Cs_nC_{60} , in which the E_F -centered flat bottom indicates vanishing electronic DOS there [Figs. 2(e), 2(f) and 3(e)–3(h)].

D. Discussion

Note that the third layer of C_{60} behaves similarly to the bilayer one in the orientational ordering and electronic structure. In what follows, we discuss the mechanism of the insulating ground states in Cs_nC_{60} fullerides with integer n . Upon doping with Cs in Cs_nC_{60} ($0 < n < 6$), the active t_{1u} orbitals with triple degeneracy are partially filled, and the simple band theory predicts a metallic character. In reality, however, the on-molecule Coulomb repulsion and JT instability, regardless of being dynamic [22,23] or static [31,45], are significant in stabilizing an insulating ground state against metallicity. The above observations of a robust insulating gap around E_F , accompanied by the satellite peaks in the electronic DOS (marked by black arrows) beyond the gaps, strongly hint at a possible lifting of the triply degenerate t_{1u} frontier orbital via JT coupling in all C_{60}^{n-} anions studied here [see the top inset of Fig. 1(e)]. Otherwise, the metal-like electronic DOS should have emerged in Cs_nC_{60} fullerides with $n = 1, 2, 4$. On the basis of JT coupling, it nowadays becomes straightforward to account for all the observed insulating ground states with the cooperative electronic correlations considered [see bottom inset of Fig. 1(e)]. In Cs_nC_{60} alkalides of even stoichiometry ($n = 2$ and 4), the strong JT coupling splits the triply degenerate LUMO states into subbands and results in a charge-disproportionated insulator [24–28], whereas in odd stoichiometries of $n = 1$ and 3 the strong electronic correlations further split one subband and lead to the Mott-insulating character. This has been well illustrated schematically by the inserted band structure in Figs. 2(d)–2(f) and 3(e)–3(h), with either lower/upper Hubbard bands (LHB/UHB) or valence/conductance bands (VB/CB) shown. Our results identify the universality of JT instability that cooperatively interplays with strong electronic correlations to stabilize the insulating states in all Cs_nC_{60} studied ($n = 1 - 4$). The strong JT coupling overcomes the intramolecular Hund's rule electron repulsion and favorably stabilizes low-spin magnetic states, matching excellently the previous reports [15,16,46]. Moreover, our observations of submolecular orientational ordering support a static nature of the JT distortions at 4.8 K, at least in the millisecond time frame of STM imaging for single C_{60} molecules [47].

Quantitatively, the energy gap Δ could be modeled as the difference between the Hubbard U and the bandwidth W in CsC_{60} and Cs_3C_{60} , whereas in Cs_2C_{60} and Cs_4C_{60} the energy separation E_{JT} between JT-split subbands becomes involved and it should be read as $\Delta = U + E_{JT} - W$ [48]. We estimate U or $U + E_{JT}$ as the energy spacing between the two DOS peaks or kinks just outside the energy gap [marked by the triangles in Figs. 2(d)–2(f) and 3(e)–3(h)] and plot them as magenta squares in the middle panels of Fig. 5(a), from which the bandwidth W could be readily extracted as well (bottom panel). As anticipated, W correlates inversely with the intermolecular spacing d [Fig. 5(b)] and faintly fluctuates between 200 and 400 meV. By contrast, U or $U + E_{JT}$ is

altered significantly with the charge state $n-$ and layer index of C_{60}^{n-} anions, being in phase with both Δ and W . This corroborates that the insulating energy gap Δ is controlled primarily by U and E_{JT} , rather than W . Compared to bilayer Cs_nC_{60} fullerides ($n = 1 - 3$), the monolayer exhibits a larger U or $U + E_{JT}$, contradicting K_nC_{60} in the Au substrate [32]. One could easily envisage this discrepancy in view of the combined screening effects from nearby polarized C_{60}^{n-} anions and the substrate. On Au(111), the substrate screening plays an essential role in Coulomb reduction, thereby leading to the smallest effective U in the monolayer [32]. However, the screening from graphene becomes negligibly small and imposes only a secondary effect on the Coulomb reduction. Alternatively, the increased nearest neighbors of C_{60}^{n-} anions from six in the monolayer to nine in the bilayer generate a more remarkable screening effect and thus smaller U , as observed. Furthermore, U in Cs_3C_{60} appears to be smaller than that in CsC_{60} because the former has higher electron doping that more effectively reduces the Coulomb repulsion. In Cs_2C_{60} and Cs_4C_{60} , both the band splitting and electronic correlations come into play; U and E_{JT} cannot be separately accessed in experiment. Nevertheless, the semiquantitative analysis explicitly reveals that the combined JT coupling and electronic correlations are responsible for the observed insulating ground states in Cs_nC_{60} fullerides.

Finally, we comment on the electronic structure in off-stoichiometric fullerides. Starting with the Cs_3C_{60} Mott insulator and charge-disproportionated Cs_4C_{60} insulator, one can easily understand the n -type and p -type behaviors in off-stoichiometric fullerides in Fig. 4 since the excess and deficiency of Cs dopants correspond to electron and hole doping, respectively. To fulfill the electronic charge neutrality, E_F is shifted upwards and downwards in monolayer Cs_3C_{60} with excess Cs and bilayer Cs_3C_{60} with Cs vacancies, resembling the doping of semiconductors [49]. Unlike atom-based semiconductors, however, the fullerene system exhibits an additional rotational degree of freedom that is fragile to doping [compare Figs. 3(d) and 4(b)]. Upon doping, the band structures, e.g., the Δ enhancement by 50 meV, might be modified as well. This accounts for the unexpectedly larger U and Δ in monolayer CsC_{60} , considering that the absent long-range orientational ordering means a deviation of doping from unity [Figs. 2(a) and 2(d)]. Indeed, the in-gap states are observed in Fig. 2(d), resembling the off-stoichiometry fullerides in Fig. 4. It is highly tempting to unravel the nature of these emergent low-lying electronic states because they might prompt metallicity or even superconductivity in Cs-doped fullerides.

IV. CONCLUSIONS

Our real-space imaging and spectroscopy of Cs-doped fullerides have established a unique correspondence among the doping level, molecular orientational ordering, and electronic structure on the submolecular scale. The insulating ground states are invariably observed for integer filling and have their roots in the combined effects of JT coupling and electronic correlations. Additional electron and hole doping shifts E_F upwards and downwards, accompanied by emergent in-gap states. The revealed similarity and distinction between the

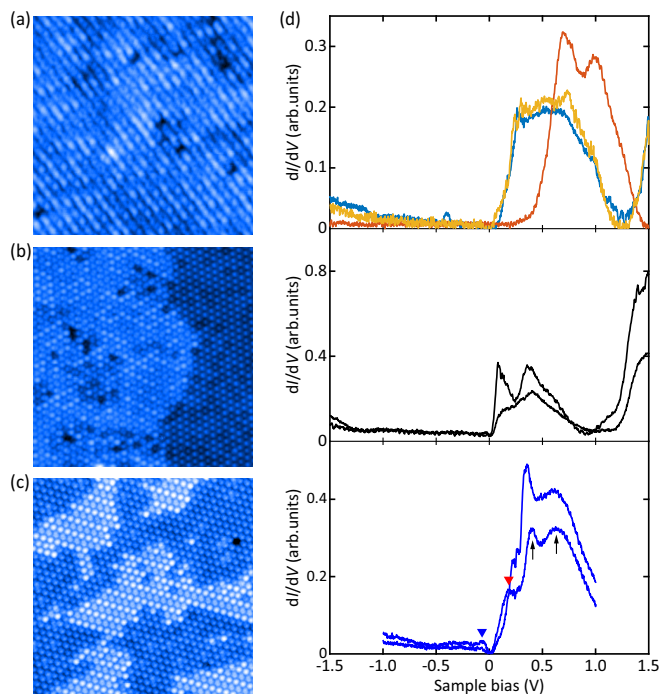


FIG. 6. Inhomogeneity and phase separation in fulleride films. (a)–(c) STM topographies ($V = 1.0$ V, $I = 100$ pA) of bilayer C_{60} with nominal Cs doping of 0.06, 0.4, and 0.9, respectively. Image size: (a) 20×20 nm² and (b) and (c) 30×30 nm². At a sufficient doping of Cs, a phase separation occurs and is characterized by bright and dark regions. (d) Spatial-dependent tunneling dI/dV spectra on $Cs_{0.06}C_{60}$ (top panel) and the bright (middle panel) and dark (bottom panel) regions of bilayer $Cs_{0.4}C_{60}$. Black and red arrows mark discrete DOS peaks caused by JT distortions and Coulomb interaction. The set point is stabilized at $V = 3.0$ V and $I = 200$ pA.

doping of fullerene and conventional semiconductors have general validity in other organic semiconductors and call for further experimental study to optimize superconductivity or other electronic properties.

ACKNOWLEDGMENTS

The work is financially supported by the Ministry of Science and Technology of China (Grants No.

2017YFA0304600, No. 2016YFA0301004, No. 2018YFA0305603), the National Natural Science Foundation of China (Grants No. 11774192, No. 11427903, No. 11634007), and in part by the Beijing Innovation Center for Future Chips, Tsinghua University.

APPENDIX: PHASE SEPARATION AND STOICHIOMETRY CONTROL

We start with the noninteger filled fullerides to track the doping dependence of STM topographies and differential conductance dI/dV spectra. Figures 6(a)–6(c) depict the representative STM images of bilayer C_{60} with a nominal Cs doping of 0.06, 0.4, and 0.9, respectively. Evidently, the doping leads to great spatial inhomogeneity and phase separation. At $n \sim 0.06$, destruction of the quasi- (2×2) superstructure is apparent, followed by the emergence of spatial inhomogeneity in dI/dV spectra [top panel of Fig. 6(d)]. The LUMO electronic states at certain positions are shifted downwards (or, equivalently, an upwards shifting of E_F), consistent with electron doping by Cs. As the doping is further increased, one can see that the STM topographies are divided into two distinct regions [Figs. 6(b) and 6(c)]. Both molecular and electronic structures in the bright regions are in analogy with those in Fig. 6(a), except for a larger upwards shifting of E_F [middle panel of Fig. 6(d)]. On the other hand, the dark regions are characteristic of more ordered molecular orientations and increase in area with Cs doping. The corresponding dI/dV spectra present a fundamental difference from those of bright regions. A new energy gap is opened around E_F , as is evident in the bottom panel of Fig. 2(d). Together with the discrete DOS peaks just above E_F that are probably due to the JT splitting of the t_{1u} orbital (marked by the black arrows), we can comprehend the gap opening (separated by the red arrows) as a consequence of strong Coulomb interactions, as detailed in the main text. This hints that the dark regions with submolecular orientational ordering correspond to a stoichiometric composition of CsC_{60} . Indeed, a sequence of molecular orientational orders is found and becomes dominant at the nominal Cs doping $n = 1$ –4, as summarized in Figs. 2 and 3. This enables us to tune the stoichiometry of Cs_nC_{60} fullerides and study their electronic structures.

- [1] A. F. Hebard, M. J. Rosseinsky, R. C. Haddon, D. W. Murphy, S. H. Glarum, T. T. M. Palstra, A. P. Ramirez, and A. R. Karton, Potassium-doped C_{60} , *Nature (London)* **350**, 600 (1991).
- [2] R. Mitsuhashi, Y. Suzuki, Y. Yamanari, H. Mitamura, T. Kambe, N. Ikeda, H. Okamoto, A. Fujiwara, M. Yamaji, N. Kawasaki, Y. Maniwa, and Y. Kubozono, Superconductivity in alkali-metal-doped picene, *Nature (London)* **464**, 76 (2010).
- [3] A. Ardavan, S. Brown, S. Kagoshima, K. Kanoda, K. Kuroki, H. Mori, M. Ogata, S. Uji, and J. Wosnitza, Recent topics of organic superconductors, *J. Phys. Soc. Jpn.* **81**, 011004 (2011).
- [4] Y. Kubozono, R. Eguchi, H. Goto, S. Hamao, T. Kambe, T. Terao, S. Nishiyama, L. Zheng, X. Miao, and H. Okamoto,

Recent progress on carbon-based superconductors, *J. Phys.: Condens. Matter* **28**, 334001 (2016).

- [5] P.-M. Allemand, K. C. Khemani, A. Koch, F. Wudl, K. Holczer, S. Donovan, G. Grüner, and J. D. Thompson, Organic molecular soft ferromagnetism in a fullerene C_{60} , *Science* **253**, 301 (1991).
- [6] Y. C. Chen, J. L. Liu, L. Ungur, J. Liu, Q. W. Li, L. F. Wang, Z. P. Ni, L. F. Chibotaru, X. M. Chen, and M. L. Tong, Symmetry-supported magnetic blocking at 20 K in pentagonal bipyramidal Dy(III) single-ion magnets, *J. Am. Chem. Soc.* **138**, 2829 (2016).
- [7] D. S. Chow, F. Zamborszky, B. Alavi, D. J. Tantillo, A. Baur, C. A. Merlic, and S. E. Brown, Charge Ordering in the TMTTF

- Family of Molecular Conductors, *Phys. Rev. Lett.* **85**, 1698 (2000).
- [8] P. A. Heiney, J. E. Fischer, A. R. McGhie, W. J. Romanow, A. M. Denenstien, J. P. McCauley, Jr., A. B. Smith, and D. E. Cox, Orientational Ordering Transition in Solid C_{60} , *Phys. Rev. Lett.* **66**, 2911 (1991).
- [9] Y. Y. Wang, R. Yamachika, A. Wachowiak, M. Grobis, K. H. Khoo, D.-H. Lee, S. G. Louie, and M. F. Crommie, Novel Orientational Ordering and Reentrant Metallicity in K_xC_{60} Monolayers for $3 \leq x \leq 5$, *Phys. Rev. Lett.* **99**, 086402 (2007).
- [10] F. Rossel, M. Pivetta, F. M. C. Patthey, E. Čavar, A. P. Seitsonen, and W. D. Schneider, Growth and characterization of fullerene nanocrystals on NaCl/Au(111), *Phys. Rev. B* **84**, 075426 (2011).
- [11] L. Tang and Q. M. Guo, Orientational ordering of the second layer of C_{60} molecules on Au(111), *Phys. Chem. Chem. Phys.* **14**, 3323 (2012).
- [12] M. Jung, D. Shin, S. D. Sohn, S. Y. Kwon, N. Park, and H. J. Shin, Atomically resolved orientational ordering of C_{60} molecules on epitaxial graphene on Cu(111), *Nanoscale* **6**, 11835 (2014).
- [13] C. D. Dimitrakopoulos and P. R. L. Malenfant, Organic thin film transistors for large area electronics, *Adv. Mater.* **14**, 99 (2002).
- [14] A. Y. Ganin, Y. Takabayashi, Y. Z. Khimiyak, S. Margadonna, A. Tamai, M. J. Rosseinsky, and K. Prassides, Bulk superconductivity at 38 K in a molecular system, *Nat. Mater.* **7**, 367 (2008).
- [15] Y. Takabayashi, A. Y. Ganin, P. Jeglič, D. Arčon, T. Takano, Y. Iwasa, Y. Ohishi, M. Takata, N. Takeshita, K. Prassides, and M. J. Rosseinsky, The disorder-free non-bcs superconductor Cs_3C_{60} emerges from an antiferromagnetic insulator parent state, *Science* **323**, 1585 (2009).
- [16] A. Y. Ganin, Y. Takabayashi, P. Jeglič, D. Arčon, A. Potočnik, P. J. Baker, Y. Ohishi, M. T. McDonald, M. D. Tzirakis, A. McLennan, G. R. Darling, M. Takata, M. J. Rosseinsky, and K. Prassides, Polymorphism control of superconductivity and magnetism in Cs_3C_{60} close to the Mott transition, *Nature (London)* **466**, 221 (2010).
- [17] P. Wzietek, T. Mito, H. Alloul, D. Pontiroli, M. Aramini, and M. Riccò, NMR Study of the Superconducting Gap Variation near the Mott Transition in Cs_3C_{60} , *Phys. Rev. Lett.* **112**, 066401 (2014).
- [18] R. H. Zadik, Y. Takabayashi, G. Klupp, R. H. Colman, A. Y. Ganin, A. Potočnik, P. Jeglič, D. Arčon, P. Matus, K. Kamarás, Y. Kasahara, Y. Iwasa, A. N. Fitch, Y. Ohishi, G. Garbarino, K. Kato, M. J. Rosseinsky, and K. Prassides, Optimized unconventional superconductivity in a molecular Jahn-Teller metal, *Sci. Adv.* **1**, e1500059 (2015).
- [19] Y. Nomura, S. Sakai, M. Capone, and R. Arita, Unified understanding of superconductivity and Mott transition in alkali-doped fullerides from first principles, *Sci. Adv.* **1**, e1500568 (2015).
- [20] Y. Takabayashi and K. Prassides, Unconventional high- t_c superconductivity in fullerides, *Philos. Trans. R. Soc. A* **374**, 20150320 (2016).
- [21] B. Keimer, S. A. Kivelson, M. R. Norman, S. Uchida, and J. Zaanen, From quantum matter to high-temperature superconductivity in copper oxides, *Nature (London)* **518**, 179 (2015).
- [22] G. Klupp, P. Matus, K. Kamarás, A. Y. Ganin, A. McLennan, M. J. Rosseinsky, Y. Takabayashi, M. T. McDonald, and K. Prassides, Dynamic Jahn-Teller effect in the parent insulating state of the molecular superconductor Cs_3C_{60} , *Nat. Commun.* **3**, 912 (2012).
- [23] A. Potočnik, A. Y. Ganin, Y. Takabayashi, M. McDonald, I. Heinmaa, P. Jeglič, R. Stern, M. Rosseinsky, K. Prassides, and D. Arčon, Jahn-Teller orbital glass state in the expanded FCC Cs_3C_{60} fulleride, *Chem. Sci.* **5**, 3008 (2014).
- [24] A. Ceulemans, L. F. Chibotaru, and F. Cimpoeu, Intramolecular Charge Disproportionation and the Band Structure of A_3C_{60} Superconductors, *Phys. Rev. Lett.* **78**, 3725 (1997).
- [25] N. Iwahara and L. F. Chibotaru, Orbital disproportionation of electronic density is a universal feature of alkali-doped fullerides, *Nat. Commun.* **7**, 13093 (2016).
- [26] S. Hoshino and P. Werner, Spontaneous Orbital-Selective Mott Transitions and the Jahn-Teller Metal of A_3C_{60} , *Phys. Rev. Lett.* **118**, 177002 (2017).
- [27] K. Ishigaki, J. Nasu, A. Koga, S. Hoshino, and P. Werner, Spontaneously orbital-selective superconductivity in a three-orbital hubbard model, *Phys. Rev. B* **98**, 235120 (2018).
- [28] A. Isidori, M. Berović, L. Fanfarillo, L. de' Medici, M. Fabrizio, and M. Capone, Charge Disproportionation, Mixed Valence, and Janus Effect in Multiorbital Systems: A Tale of Two Insulators, *Phys. Rev. Lett.* **122**, 186401 (2019).
- [29] W. Yang, V. Brouet, X. Zhou, H. J. Choi, S. G. Louie, M. L. Cohen, S. Kellar, P. Bogdanov, A. Lanzara, A. Goldoni, F. Parmigiani, Z. Hussain, and Z. X. Shen, Band structure and fermi surface of electron-doped C_{60} monolayers, *Science* **300**, 303 (2003).
- [30] M. P. Gelfand and J. P. Lu, Orientational Disorder and Electronic States in C_{60} and A_3C_{60} , Where A Is an Alkali Metal, *Phys. Rev. Lett.* **68**, 1050 (1992).
- [31] A. Wachowiak, R. Yamachika, K. Khoo, Y. Wang, M. Grobis, D. H. Lee, S. G. Louie, and M. F. Crommie, Visualization of the molecular Jahn-Teller effect in an insulating K_4C_{60} monolayer, *Science* **310**, 468 (2005).
- [32] Y. Y. Wang, R. Yamachika, A. Wachowiak, M. Grobis, and M. F. Crommie, Tuning fulleride electronic structure and molecular ordering via variable layer index, *Nat. Mater.* **7**, 194 (2008).
- [33] D. R. Daughton and J. A. Gupta, Orientation dependence of charge transfer for C_{60} on Cu(100), *Appl. Phys. Lett.* **98**, 71 (2011).
- [34] S. I. Bozhko, S. A. Krasnikov, O. Lübben, B. E. Murphy, K. Radican, V. N. Semenov, H.-C. Wu, E. A. Levchenko, A. N. Chaika, N. N. Sergeeva, and I. V. Shvets, Correlation between charge-transfer and rotation of C_{60} on $WO_2/W(110)$, *Nanoscale* **5**, 3380 (2013).
- [35] J. Cho, J. Smerdon, L. Gao, Ö. Sützer, J. R. Guest, and N. P. Guisinger, Structural and electronic decoupling of C_{60} from epitaxial graphene on SiC, *Nano Lett.* **12**, 3018 (2012).
- [36] H. Q. Wang, C. G. Zeng, B. Wang, J. G. Hou, Q. X. Li, and J. L. Yang, Orientational configurations of the C_{60} molecules in the (2×2) superlattice on a solid $C_{60}(111)$ surface at low temperature, *Phys. Rev. B* **63**, 085417 (2001).
- [37] X. H. Lu, M. Grobis, K. H. Khoo, S. G. Louie, and M. F. Crommie, Charge transfer and screening in individual C_{60} molecules on metal substrates: A scanning tunneling spectroscopy and theoretical study, *Phys. Rev. B* **70**, 115418 (2004).
- [38] G. Schull, N. Néel, M. Becker, J. Kröger, and R. Berndt, Spatially resolved conductance of oriented C_{60} , *New J. Phys.* **10**, 065012 (2008).

- [39] A. Auerbach, N. Manini, and E. Tosatti, Electron-vibron interactions in charged fullerenes. I. Berry phases, *Phys. Rev. B* **49**, 12998 (1994).
- [40] N. Manini, E. Tosatti, and A. Auerbach, Electron-vibron interactions in charged fullerenes. II. pair energies and spectra, *Phys. Rev. B* **49**, 13008 (1994).
- [41] D. L. Huang, P. D. Dau, H. T. Liu, and L. S. Wang, High-resolution photoelectron imaging of cold C_{60}^- anions and accurate determination of the electron affinity of C_{60} , *J. Chem. Phys.* **140**, 224315 (2014).
- [42] C. Große, O. Gunnarsson, P. Merino, K. Kuhnke, and K. Kern, Nanoscale imaging of charge carrier and exciton trapping at structural defects in organic semiconductors, *Nano Lett.* **16**, 2084 (2016).
- [43] E. J. Santos, D. Scullion, X. S. Chu, D. O. Li, N. P. Guisinger, and Q. H. Wang, Rotational superstructure in van der waals heterostructure of self-assembled C_{60} monolayer on the WSe_2 surface, *Nanoscale* **9**, 13245 (2017).
- [44] J. Leaf, A. Stannard, S. P. Jarvis, P. Moriarty, and J. L. Dunn, A combined monte carlo and hückel theory simulation of orientational ordering in C_{60} assemblies, *J. Phys. Chem. C* **120**, 8139 (2016).
- [45] S. S. Naghavi, M. Fabrizio, T. Qin, and E. Tosatti, Nanoscale orbital excitations and the infrared spectrum of a molecular Mott insulator: $A15-Cs_3C_{60}$, *Nanoscale* **8**, 17483 (2016).
- [46] M. Fabrizio and E. Tosatti, Nonmagnetic molecular Jahn-Teller Mott insulators, *Phys. Rev. B* **55**, 13465 (1997).
- [47] I. D. Hands, J. L. Dunn, and C. A. Bates, Visualization of static Jahn-Teller effects in the fullerene anion C_{60}^- , *Phys. Rev. B* **82**, 155425 (2010).
- [48] R. W. Lof, M. A. van Veenendaal, B. Koopmans, H. T. Jonkman, and G. A. Sawatzky, Band Gap, Excitons, and Coulomb Interaction in Solid C_{60} , *Phys. Rev. Lett.* **68**, 3924 (1992).
- [49] T. F. Rosenbaum, R. F. Milligan, M. A. Paalanen, G. A. Thomas, R. N. Bhatt, and W. Lin, Metal-insulator transition in a doped semiconductor, *Phys. Rev. B* **27**, 7509 (1983).